

# Tests of conservation laws in post-Newtonian gravity with binary pulsars

XUELI MIAO,<sup>1</sup> JUNJIE ZHAO,<sup>1,\*</sup> LIJING SHAO,<sup>2,3</sup> NORBERT WEX,<sup>3</sup> MICHAEL KRAMER,<sup>3,4</sup> AND BO-QIANG MA<sup>1,5,6</sup>

<sup>1</sup>*School of Physics and State Key Laboratory of Nuclear Physics and Technology, Peking University, Beijing 100871, China*

<sup>2</sup>*Kavli Institute for Astronomy and Astrophysics, Peking University, Beijing 100871, China*

<sup>3</sup>*Max-Planck-Institut für Radioastronomie, Auf dem Hügel 69, D-53121 Bonn, Germany*

<sup>4</sup>*Jodrell Bank Centre for Astrophysics, The University of Manchester, Oxford Road, Manchester M13 9PL, United Kingdom*

<sup>5</sup>*Collaborative Innovation Center of Quantum Matter, Beijing, China*

<sup>6</sup>*Center for High Energy Physics, Peking University, Beijing 100871, China*

(Received January 1, 2020; Revised January 1, 2020; Accepted January 1, 2020)

Submitted to ApJ

## ABSTRACT

General relativity is a fully conservative theory, but there exist other possible metric theories of gravity. We consider non-conservative ones with a parameterized post-Newtonian (PPN) parameter,  $\zeta_2$ . A non-zero  $\zeta_2$  induces a self-acceleration for the center of mass of an eccentric binary pulsar system, which contributes to the second time derivative of the pulsar spin frequency,  $\dot{\nu}$ . In our work, using the method in Will (1992), we provide an improved analysis with four well-timed, carefully-chosen binary pulsars. In addition, we extend Will's method and derive  $\zeta_2$ 's effect on the third time derivative of the spin frequency,  $\ddot{\nu}$ . For PSR B1913+16, the constraint from  $\ddot{\nu}$  is even tighter than that from  $\dot{\nu}$ . We combine multiple pulsars with Bayesian inference, and obtain an upper limit,  $|\zeta_2| < 1.3 \times 10^{-5}$  at 95% confidence level, assuming a flat prior in  $\log_{10} |\zeta_2|$ . It improves the existing bound by a factor of three. Moreover, we propose an analytical timing formalism for  $\zeta_2$ . Our simulated times of arrival with simplified assumptions show binary pulsars' capability in limiting  $\zeta_2$ , and useful clues are extracted for real data analysis in future. In particular, we discover that for PSRs B1913+16 and J0737–3039A,  $\ddot{\nu}$  can yield more constraining limits than  $\dot{\nu}$ .

*Keywords:* gravitation – methods: statistical – binaries: general – pulsars: general

## 1. INTRODUCTION

In particle physics, conservation laws play an important role. They are default methods to analyze the scattering problem of particles, and have helped scientists in discovering new particles, e.g. neutrons and neutrinos (Chadwick 1932; Cowan et al. 1956). In the field of gravitation, conservation laws do not apply to all metric theories of gravity. Already at the first post-Newtonian level, they are violated in some gravity theories. For example, extending the Brans-Dicke theory, Smalley (1975) constructed a class of gravitational theories

with consistent field equations but non-zero divergence of the energy-momentum tensor (see also Rastall 1972).

At the first post-Newtonian order, the degree of violation of conservation laws is expressed via some specific parameterized post-Newtonian (PPN) parameters (Will 2018). In order to test the post-Newtonian gravity, we can bound the PPN parameters in a generic way. These bounds can be translated to theory parameters afterwards (Will 2018).

For a fully conservative theory, the energy, linear momentum, and angular momentum are conserved, and PPN parameters satisfy  $\alpha_1 = \alpha_2 = \alpha_3 = \zeta_1 = \zeta_2 = \zeta_3 = \zeta_4 = 0$  (Will 2018). For semi-conservative theories, the energy and linear momentum are conserved, but a preferred frame is allowed to exist, which breaks the symmetry of local Lorentz invariance (LLI) for the gravitational interaction. In these theories, PPN parameters satisfy  $\alpha_3 = \zeta_1 = \zeta_2 = \zeta_3 = \zeta_4 = 0$  (Will 2018). Empirically, the best constraints on the other two PPN parameters, namely  $\alpha_1$  and  $\alpha_2$ , respectively come from observations of the small-eccentricity binary pulsar

Corresponding author: Lijing Shao  
lshao@pku.edu.cn

Corresponding author: Norbert Wex  
wex@mpifr-bonn.mpg.de

\* The first two authors contributed equally to the work.

PSR J1738+0333 (Damour & Esposito-Farèse 1992; Freire et al. 2012; Shao & Wex 2012) and two solitary millisecond pulsars, PSRs B1937+21 and J1744–1134 (Nordtved 1987; Shao et al. 2013). Non-conservative theories violate the energy-momentum conservation laws, and one or more of  $\{\alpha_3, \zeta_1, \zeta_2, \zeta_3, \zeta_4\}$  will be non-zero (Will 2018).

In this work, we consider a class of theories with a non-zero  $\zeta_2$ . Smalley (1975) explicitly showed that  $\zeta_2$  could indeed appear non-zero in gravitational theories with non-vanishing divergence of the energy-momentum tensor. Will (1976, 1992) discovered that in these theories, the center of mass of an eccentric binary system possesses an energy-momentum-violating self-acceleration. Therefore, we can use binary pulsars to test the PPN parameter  $\zeta_2$ .

In 1974, Hulse & Taylor (1975) discovered the first binary pulsar system, PSR B1913+16. This system provided a verification of the existence of gravitational-wave radiation for the first time (Taylor et al. 1979). The orbital period decay rate,  $\dot{P}_b$ , of this system is consistent with the predicted value from general relativity (GR). Such an observational fact can be used to test the foundation of gravity. For example,  $\dot{P}_b$  was used to test if the graviton is massless (Finn & Sutton 2002; Miao et al. 2019). The high-precision results for PSR B1913+16 benefit from an extremely accurate measurement technique, the so-called *pulsar timing*. Pulsar timing models the times of arrival (TOAs) of pulses emitted from a pulsar and determines timing parameters to a high precision via fitting to a timing formula (Taylor 1992). With its help, we can use binary pulsar systems to perform various tests of gravity (Stairs 2003; Wex 2014; Shao & Wex 2016).

Until now, GR has passed all tests with flying colors (Will 2014). However, it is still important to look for gravity theories beyond GR and also to test GR more and more precisely (Berti et al. 2015). If there exist non-conservative effects in the gravitational interaction, there could be a self-acceleration for the center of mass of an eccentric binary system (Will 1976, 1992). It leads to abnormal changes in the observed pulsar spin and orbital periods. Therefore, we can use binary pulsar systems to perform gravitational tests and constrain the corresponding PPN parameters. Note that such constraints on PPN parameters are in the strong-field regime, because neutron stars are strongly self-gravitating objects. Tests with binary pulsars are therefore sensitive to strong-field modifications of the weak field PPN parameter  $\zeta_2$ .<sup>1</sup> The latest bound on  $\zeta_2$  was obtained by Will (1992). He used the second time derivative of the spin period (namely  $\ddot{P}$ ) of PSR B1913+16, and limited  $\zeta_2$  to be smaller than  $4 \times 10^{-5}$  at 95% confidence level (C.L.). Worth to note that,

the value of  $\ddot{P}$ , used by Will (1992), was evidently obtained from unpublished work by J. H. Taylor and colleagues, but more recent data give a less constraining bound (Weisberg & Huang 2016b). This might have been caused by the existence of red noise, which over a long timing baseline can mimic higher-order spin period derivatives. It makes the bound over-optimistic by more than an order of magnitude. Therefore, we shall treat the limit in Will (1992) as an optimistic one.

In this paper, we perform an improved analysis of binary pulsars to constrain the strong-field counterpart of the PPN parameter  $\zeta_2$ . First, using the method in Will (1992), we utilize four carefully chosen binary pulsar systems to constrain  $\zeta_2$ , including PSR B1913+16 with the updated data. The analysis depends on the value of the longitude of periastron,  $\omega$ . We attempt to include the effect from the relativistic periastron advance of the orbit, which renders the value of  $\omega$  as a linear function of time, and the time variation appears to be significant for some systems. We adopt two methods to constrain  $\zeta_2$  with different choices of  $\cos \omega(t)$ , where  $\omega(t)$  is the time-dependent longitude of periastron. In both cases, the best bound with an individual binary pulsar is from PSR B2127+11C (Jacoby et al. 2006, Ridolfi et al. in preparation),

$$|\zeta_2| \lesssim 3 \times 10^{-5} \quad (95\% \text{ C.L.}). \quad (1)$$

It is already tighter than the previous best bound obtained from PSR B1913+16 (Will 1992).

In addition, we extend Will's method and derive the relation between the third time derivative of the spin frequency,  $\ddot{\nu}$ , and  $\zeta_2$ . Notice that, in this work, we will use time derivatives of the pulsar spin frequency,  $\dot{\nu}$  and  $\ddot{\nu}$ , instead of time derivatives of the pulsar spin period,  $\dot{P}$  and  $\ddot{P}$ , that were used by Will (1992). These two approaches are equivalent after properly accounting for the chain rule in taking time derivatives. In pulsar timing, the use of frequency derivatives yields a simpler description of the pulsar's spin phase versus time, and it is widely adopted. In our analysis, the values of  $\ddot{\nu}$  are attainable for PSRs B1913+16 and B1534+12, and they are used to bound  $\zeta_2$ . Interestingly, for PSR B1913+16, the constraint from  $\ddot{\nu}$  is even tighter than that from  $\dot{\nu}$ .

With a coherent approach of the Bayesian inference, we combine individual bounds from four binary pulsars. We obtain a combined bound with a prior uniform in  $\log_{10} |\zeta_2|$ ,

$$|\zeta_2| < 1.3 \times 10^{-5} \quad (95\% \text{ C.L.}). \quad (2)$$

It improves Will (1992)'s limit by a factor of three.

Moreover, we develop, for the first time, a timing formula that includes  $\zeta_2$ . We use it to investigate the capability of limiting  $\zeta_2$  from individual binary pulsars. We simulate TOAs for each pulsar with the effect of  $\zeta_2$  included, and investigate the ability to constrain  $\zeta_2$ . If the effect of  $\zeta_2$  is smaller than

<sup>1</sup> In the absence of non-perturbative phenomena, one could think of an expansion in terms of the compactnesses  $C_i$  of the pulsar and its companion:  $\zeta_2 = \zeta_2^{\text{PPN}} + a_i C_i + a_{ij} C_i C_j + \dots$

the sensitivity of a system to it (which depends on the orbital characteristics and TOA accuracy), then the  $\zeta_2$  can not be measured. It is shown that, if there were only white Gaussian noise, as it is in our simulation, the Hulse-Taylor pulsar PSR B1913+16 would achieve the tightest upper limit, due to its long observational span and small timing residuals. However, the existence of red noise in data will deteriorate the test in reality. Interestingly, in this new method, we find as well that for PSRs B1913+16 and J0737–3039A, the third time derivative of the spin frequency,  $\ddot{\nu}$ , can yield a stronger constraint on  $\zeta_2$  than  $\dot{\nu}$ .

The paper is organized as follows. In the next section, we briefly review the binary dynamics with the PPN parameter  $\zeta_2$ . In Section 3, using an improved method of Will (1992), we calculate the  $\zeta_2$  bounds from four binary pulsars individually. Then, by including all four pulsars in the Bayesian inference, we obtain a combined bound on  $\zeta_2$ . In Section 4, we develop a new timing formula and simulate TOAs with the contribution of  $\zeta_2$ . We show the ability to limit  $\zeta_2$  from different pulsars based on their current observational characteristics. Though the simulations are oversimplified with white Gaussian noise and uniform cadence, they still provide some useful clues for future analysis with real data. We summarize our results in Section 5.

## 2. BINARY PULSARS WITH PPN $\zeta_2$

For non-conservative gravity theories with the PPN parameter  $\zeta_2$ , there exists a self-acceleration for the center of mass of a binary system (Will 1976, 1992). The extra acceleration vector reads,

$$\mathbf{a}_{\text{cm}}(t) = \frac{\zeta_2}{2} c T_{\odot} m_c \frac{q(q-1)}{(1+q)^2} \left( \frac{2\pi}{P_b} \right)^2 \frac{e}{(1-e^2)^{3/2}} \hat{\mathbf{e}}_p(t), \quad (3)$$

where,  $m_p$  and  $m_c$  are respectively the masses for the pulsar and its companion star in the Solar unit;  $q \equiv m_p/m_c$  is the mass ratio;  $P_b$  is the orbital period, and  $e$  is the orbital eccentricity;  $\hat{\mathbf{e}}_p(t)$  is a unit vector directed from the center of mass of the system to the point of periastron of the pulsar;  $c$  is the speed of light, and  $T_{\odot} \equiv GM_{\odot}/c^3 \simeq 4.9254909 \mu\text{s}$  with  $M_{\odot}$  denoting the Solar mass (Mamajek et al. 2015). In addition to  $\zeta_2$ , other PPN parameters may as well contribute to Eq. (3), but they have been constrained tightly (Will 2014, 2018). In this work, we focus on the impact of  $\zeta_2$ .

The self-acceleration (3) for the center of mass of a binary system signals a violation of post-Newtonian energy-momentum conservation (Will 1976, 1992). It leads to a *changing* Doppler shift between the Solar system and the binary pulsar system, due to a uniform rotation of  $\hat{\mathbf{e}}_p(t)$  caused by the relativistic periastron advance. This effect changes the *observed* pulsar spin and orbital frequencies (Will 1976, 1992). In this work, we only consider the  $\zeta_2$ -induced change in the spin frequency. This change can be described via

$\dot{\nu}/\nu \approx -\mathbf{a}_{\text{cm}} \cdot \hat{\mathbf{n}}/c$ , where  $\hat{\mathbf{n}}$  is a unit vector along the line of sight to the binary. The change of the pulsar spin frequency,  $\dot{\nu}$ , is generally degenerate with its intrinsic spindown value (Lorimer & Kramer 2005). Therefore, we turn to the change of the second time derivative,  $\ddot{\nu}$ , which is caused by the changing orientation of  $\hat{\mathbf{e}}_p(t)$  (thus,  $\mathbf{a}_{\text{cm}}$ ), due to the advance of the periastron in GR for a relativistic binary.

If we assume that  $\dot{\nu}$  is entirely from the contribution of  $\dot{\mathbf{a}}_{\text{cm}}$ , the relation between  $\ddot{\nu}$  and  $\zeta_2$  is,

$$\frac{1}{\nu} \frac{d^2 \nu}{dt^2} = -\frac{\mathcal{A}_2}{c} \cos \omega \frac{d\omega}{dt}, \quad (4)$$

where

$$\mathcal{A}_2 \equiv -\frac{\zeta_2}{2} c T_{\odot} \left( \frac{2\pi}{P_b} \right)^2 \frac{q(q-1)}{(1+q)^2} \frac{e}{(1-e^2)^{3/2}} m_c \sin i. \quad (5)$$

For convenience, we make use of the mass function,

$$m_c \sin i = (\mathcal{G} M_{\odot})^{-1/3} \left( \frac{2\pi m}{P_b} \right)^{2/3} a_p \sin i. \quad (6)$$

In above three equations,  $\omega$  is the longitude of periastron,  $m \equiv m_p + m_c$  is the total mass of the binary system in the unit of  $M_{\odot}$ ,  $i$  is the orbital inclination and  $(a_p/c) \sin i \equiv x_p$  is the projected semi-major axis of the pulsar orbit. Though the *effective* gravitational constant  $\mathcal{G}$  in principle could deviate from its Newtonian counterpart  $G$ , in particular in the presence of strongly self-gravitating bodies, they were constrained to be close from several pulsar systems (Shao & Wex 2016). Therefore, we safely take  $\mathcal{G} = G$  in our calculation as an approximation. By inverting Eq. (4), it is straightforward to see that, if  $e$  and  $\dot{\omega}$  are large enough, and  $|q-1|$  does not vanish, a limit of  $\zeta_2$  can be obtained using the measurement of  $\ddot{\nu}$ .

The second time derivative of spin frequency (4) is equivalent to Eq. (3) in Will (1992) for the second time derivative of spin period, after dropping negligible higher-order terms. Will (1992) chose the second time derivative of the spin period of PSR B1913+16 to constrain  $\zeta_2$ , and he got a tight bound,  $|\zeta_2| < 4 \times 10^{-5}$  at 95% C.L.. In this work, we largely follow the spirit of Will (1992), while making several improvements to his method.

Besides the  $\dot{\nu}$  test, we extend Will's work to bound  $\zeta_2$  with the third time derivative of the pulsar spin frequency,  $\ddot{\nu}$ , and investigate what kind of constraint can be obtained from it. We derive the relation between  $\ddot{\nu}$  and  $\zeta_2$  by using the same method in the Appendix of Will (1992). After dropping higher-order contributions, we get,

$$\frac{1}{\nu} \frac{d^3 \nu}{dt^3} = \frac{\mathcal{A}_2}{c} \sin \omega \left( \frac{d\omega}{dt} \right)^2. \quad (7)$$

## 3. NEW LIMITS ON $\zeta_2$

In this section, we apply Will’s method (Will 1992) to the latest published parameters of four binary pulsars, in order to place updated bounds on the PPN parameter  $\zeta_2$ . In Section 3.1, we show our strategy to choose binary pulsar systems with high figure of merit. In Section 3.2 the latest parameters of four binary pulsars are made use of to constrain  $\zeta_2$  from individual binary pulsars. We stack them to obtain a combined bound on  $\zeta_2$  with the Bayesian inference in Section 3.3.

### 3.1. Selection of binary pulsars

Because of its small timing residuals and a long observational time span for decades, the Hulse-Taylor pulsar PSR B1913+16 bounded  $\zeta_2$  tightly (Will 1992). However, now we have many more relativistic binary pulsars (Wex 2014; Manchester 2015), which have potential to provide stronger bounds on  $\zeta_2$ . We make use of the latest published results of binary pulsars, and update the bound of  $\zeta_2$  with improved methods.

We select binary pulsars from the ATNF pulsar catalog<sup>2</sup> (Manchester et al. 2005) in the hope to include all potential binary pulsars with high figure of merit. First, we choose binary pulsars who have measured values of  $e$ ,  $\dot{\nu}$ ,  $x_p$ ,  $\omega$ , and  $\dot{\omega}$ , which are the parameters appearing in Eq. (4). Particularly, we select relativistic binary systems with  $\dot{\omega} > 0.03^\circ \text{ yr}^{-1}$ . The eligible systems are PSRs B2127+11C (Jacoby et al. 2006), B1534+12 (Fonseca et al. 2014), B1802–07 (Hobbs et al. 2004), J1906+0746 (van Leeuwen et al. 2015), J0024–7204U, J0024–7204S, B0021–72H, and B0021–72E (Freire et al. 2017). We obtain approximate constraints on  $\zeta_2$  from these systems by setting  $\cos \omega = 1$  for a rough estimation. We find that, only PSRs B2127+11C and B1534+12 have the potential to constrain  $\zeta_2$  to an interesting level. We collect relevant parameters of PSRs B2127+11C and B1534+12 in Table 1. For PSR B2127+11C we have listed updated values for  $\dot{\nu}$  and masses from Ridolfi et al. (in preparation). We also include PSR B1913+16 in Table 1. In the latest publication, Weisberg & Huang (2016b) did not report the measurement of  $\dot{\nu}$ , but we can access relevant TOAs and associated online data from Weisberg & Huang (2016a). We use TEMPO<sup>3</sup> to obtain the value of  $\dot{\nu}$  for PSR B1913+16. Moreover, we include PSR J1756–2251 in Table 1, whose  $\dot{\nu}$  was provided by R. Ferdman (private communication), by using the data in Ferdman et al. (2014). We also tried to use an approximate formula in Shao (2014a,b) to estimate the value of  $\dot{\nu}$  from the uncertainty of  $\dot{\nu}$ . The approximate formula works well for time derivatives of orbital elements (Shao & Bailey 2018), but is too optimistic for the spin parameters. This might be

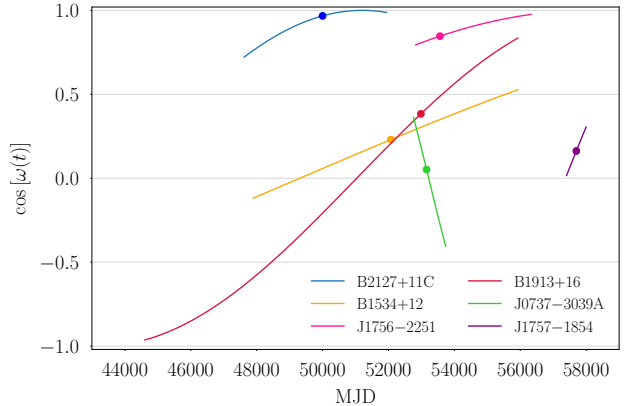


**Figure 1.** The cosines of the longitude of periastron for six binary pulsars in Tables 1 and 3, during their observational spans that were used to derive the timing solution. The dots denote the reference epoch for the timing parameters.

due to the characteristics of timing uncertainties, in particular in the presence of red timing noise. Therefore, we do not include the estimation in the calculation.

In a short summary, we have collected four binary pulsars in Table 1 to investigate possible constraints on  $\zeta_2$ .

### 3.2. Individual bounds on $\zeta_2$

We use  $\dot{\nu}$  in Eq. (4) for four binary pulsars to obtain individual bounds on  $\zeta_2$ . However, we shall notice that, there could exist some other effects which contribute to  $\dot{\nu}$ . Thus they should be subtracted before testing  $\zeta_2$ . It is generally thought that pulsars have strong dipole magnetic fields. A rotating pulsar leads to the emission of electromagnetic waves which causes its spindown. The corresponding  $\dot{\nu}^{\text{dipole}}$  can be calculated from the magnetic dipole braking formula,  $\dot{\nu}^{\text{dipole}} = n\dot{\nu}^2/\nu$ , where  $\nu$  is the spin frequency of the pulsar and  $n$  is the so-called braking index (Lorimer & Kramer 2005). For those binary pulsar systems, the values of  $\dot{\nu}^{\text{dipole}}$  are calculated and listed in Table 1, assuming  $n = 3$  for a dominant magnetic dipole braking. We find that, when compared with the measured  $\dot{\nu}$ , the contribution from the magnetic dipole braking,  $\dot{\nu}^{\text{dipole}}$ , is two orders of magnitude smaller. Therefore, it can be neglected safely when we constrain the PPN parameter  $\zeta_2$  using  $\dot{\nu}$ . Other values of the braking index  $n$  give a similar result. Besides the magnetic braking, the environment of globular clusters and possible nearby masses (Joshi & Rasio 1997) could also contribute to the time derivatives of the spin frequency. Usually cluster potential will not lead to significant  $\dot{\nu}$  and  $\ddot{\nu}$ . For nearby small-mass objects (e.g. in the PSR B1620–26 system), it is very unlikely to conspire with  $\zeta_2$  to cancel the effect completely. As for the time derivative of the Galactic acceleration to the binary pulsar system, we use the data from Weisberg et al. (2008) and Weisberg & Huang (2016b) to derive

<sup>2</sup> <https://www.atnf.csiro.au/research/pulsar/psrcat>

<sup>3</sup> <http://tempo.sourceforge.net>

**Table 1.** Relevant parameters for PSRs B2127+11C (Jacoby et al. 2006), B1534+12 (Fonseca et al. 2014), B1913+16 (Weisberg & Huang 2016b), and J1756–2251 (Ferdman et al. 2014). Their  $\dot{\nu}$  was obtained from pulsar timing data directly. The  $\dot{\nu}$  for PSR J1756–2251 was provided by R. Ferdman (private communication) using data in Ferdman et al. (2014), and we use updated  $\dot{\nu}$  and masses for PSR B2127+11C from Ridolfi et al. (in preparation). Binary masses were obtained assuming the validity of GR. The contribution to  $\dot{\nu}$  from the magnetic dipole braking,  $\dot{\nu}^{\text{dipole}}$ , is calculated assuming a braking index  $n = 3$ . Parenthesized numbers represent the 1- $\sigma$  uncertainty in the last digit(s) quoted.

	PSR B2127+11C	PSR B1534+12	PSR B1913+16	PSR J1756–2251
Reference time, $t_0$ (MJD)	50000	52077	52984	53563
Observational span, $T^{\text{obs}}$ (yr)	$\sim 12$	$\sim 22$	$\sim 31$	$\sim 9.6$
Spin frequency, $\nu$ (Hz)	32.755422697308(11)	26.38213277689397(11)	16.940537785677(3)	35.1350727145469(6)
First derivative of $\nu$ , $\dot{\nu}$ ( $\text{s}^{-2}$ )	$-5.35160(3) \times 10^{-15}$	$-1.686097(2) \times 10^{-15}$	$-2.4733(1) \times 10^{-15}$	$-1.256079(3) \times 10^{-15}$
Second derivative of $\nu$ , $\ddot{\nu}$ ( $\text{s}^{-3}$ )	$2.7(26) \times 10^{-28}$	$1.70(11) \times 10^{-29}$	$1.59(15) \times 10^{-26}$	$-2.4(1) \times 10^{-27}$
Third derivative of $\nu$ , $\dddot{\nu}$ ( $\text{s}^{-4}$ )	–	$-1.6(2) \times 10^{-36}$	$-5.0(7) \times 10^{-35}$	–
$\dot{\nu}^{\text{dipole}}$ ( $\text{s}^{-3}$ )	$2.6 \times 10^{-30}$	$3.2 \times 10^{-31}$	$1.0 \times 10^{-30}$	$1.3 \times 10^{-31}$
Orbital period, $P_b$ (day)	0.33528204828(5)	0.420737298879(2)	0.322997448918(3)	0.31963390143(3)
Eccentricity, $e$	0.681395(2)	0.27367752(7)	0.6171340(4)	0.1805694(2)
Projected semi-major axis, $x_p$ (lt-s)	2.51845(6)	3.7294636(6)	2.341776(2)	2.756457(9)
Longitude of periastron, $\omega$ (deg)	345.3069(5)	283.306012(12)	292.54450(8)	327.8245(3)
Periastron advance, $\dot{\omega}$ ( $\text{deg yr}^{-1}$ )	4.4644(1)	1.7557950(19)	4.226585(4)	2.58240(4)
Pulsar mass, $m_p$ ( $M_\odot$ )	1.3518(9)	1.3330(2)	1.438(1)	1.341(7)
Companion mass, $m_c$ ( $M_\odot$ )	1.3610(9)	1.3455(2)	1.390(1)	1.230(7)
Mass ratio, $q \equiv m_p/m_c$	0.993(1)	1.0094(2)	1.0345(10)	1.090(8)
Number of TOAs, $N_{\text{TOA}}$	631	9897	9257	8743
RMS timing residual, $\sigma_{\text{TOA}}$ ( $\mu\text{s}$ )	26.0	4.57	17.5	19.3

a rough estimation for PSR B1913+16. We obtain that such an effect contributes to  $\dot{\nu}$  at the level of  $10^{-33} \text{ s}^{-3}$ , far less than the observed  $\dot{\nu} \sim 10^{-26} \text{ s}^{-3}$ . Therefore, the effect from a time-varying Galactic acceleration can be ignored as well.

We use the parameters of selected binary systems in Table 1 to place updated bounds on  $\zeta_2$  with Eq. (4). For a parameter  $Y \in \{\nu, P_b, e, x_p, \dot{\omega}, q, m\}$ , in the calculation we take its measured value and associated 1- $\sigma$  uncertainty,  $\sigma(Y)$ . We generate parameters randomly with a normal distribution  $\mathcal{N}[Y, \sigma^2(Y)]$ . In principle, some of these parameters should change over the observational time span. For example, the gravitational-wave radiation causes  $P_b(t) \approx P_b(t_0) + \dot{P}_b(t - t_0)$ . We have checked that, these time-varying changes are negligible in putting bounds on  $\zeta_2$ . Therefore, we directly adopt the values at the reported reference time for simplicity, with the exception of  $\omega$  (see below).

For the key parameter,  $\dot{\nu}$ , to be on the conservative side, we randomly generate with a normal distribution  $\mathcal{N}[0, \sigma^2(\dot{\nu}^{\text{upper}})]$ , where,  $\sigma(\dot{\nu}^{\text{upper}})$  is the upper limit of  $\dot{\nu}$  from  $\zeta_2$ . For the four systems in Table 1, we conservatively use  $\sigma^2(\dot{\nu}^{\text{upper}}) = \dot{\nu}^2 + \sigma^2(\dot{\nu})$ . This treatment is the most conservative, only assuming that there is no extremely fortuitous cancellation against  $\zeta_2$  with opposite signs from other contributing sources to  $\dot{\nu}$ .

For some relativistic binary pulsars, the periastron advance is large enough to be measurable. For example, the Hulse-Taylor pulsar has  $\dot{\omega} \approx 4.2^\circ \text{ yr}^{-1}$  (Weisberg & Huang 2016b) and the Double Pulsar has  $\dot{\omega} \approx 17^\circ \text{ yr}^{-1}$  (Kramer et al. 2006). In order to have a  $90^\circ$  change in  $\omega$ , the Hulse-Taylor pulsar and the Double pulsar need  $\sim 20 \text{ yr}$  and  $\sim 5 \text{ yr}$  respectively. We note that, in our test there is a  $\cos[\omega(t)]$  term in Eq. (4). It indicates that, differently from other parameters, the longitude of periastron  $\omega$  can vary greatly over the observational span, thus affecting the  $\zeta_2$  test. The observational spans for binary pulsars in Table 1 are of years to decades, which lead to significant changes in  $\omega$  and  $\cos[\omega(t)]$ . Figure 1 shows the evolution of  $\cos[\omega(t)]$  for binary pulsars over their observational span  $T^{\text{obs}}$ .

For some binary systems,  $\cos[\omega(t)]$  crosses zero during some epoch, indicating a loose constraint on  $\zeta_2$  via Eq. (4). Consequently, we should treat the value of  $\cos[\omega(t)]$  with great caution. In Will (1992),  $|\cos[\omega(t)]| = 0.5$  was chosen for PSR B1913+16. In our analysis, two different methods for calculating  $\zeta_2$  are used:

- **METHOD A:** for each pulsar, we uniformly take the value of  $\omega(t)$  during its real observational span. The corresponding distribution of  $\cos[\omega(t)]$  is used in our Monte Carlo calculation.

- **METHOD B:** for each pulsar, we use the value of  $\cos[\omega(t)]$  at the reference time  $t_0$ , denoted as dots in Fig. 1. This reference time is usually chosen to be close to the mid-point of the whole observation.

Plugging the distribution of  $\cos[\omega(t)]$  and the distributions of other relevant parameters with their due uncertainties into Eq. (4), we collect the distribution of  $\zeta_2$  for statistical inference. We find that, the distribution of  $\zeta_2$  has a mean value that is very close to zero. We take the symmetric range enclosing 95% posteriors as the upper limit of  $\zeta_2$  from the distribution. The corresponding upper limits from different binaries with **METHOD A** and **METHOD B** are given in Table 2.

In our selection of binary pulsars, only two have reported  $\ddot{\nu}$  in their published timing solution. They are PSRs B1534+12 (Fonseca et al. 2014) and B1913+16 (Weisberg & Huang 2016a,b). In particular, we have used the TEMPO software to get the value of  $\ddot{\nu}$  for PSR B1913+16 from their published online data (Weisberg & Huang 2016a). The values of  $\ddot{\nu}$  for these two pulsars are listed in Table 1. Similar to the previous calculation, we randomly generate a normal distribution for  $\ddot{\nu}$  with  $\mathcal{N}[0, \sigma^2(\ddot{\nu}^{\text{upper}})]$ , where  $\sigma^2(\ddot{\nu}^{\text{upper}}) = \ddot{\nu}^2 + \sigma^2(\ddot{\nu})$ . We utilize **METHOD A** and **METHOD B** to obtain the value of  $\omega(t)$ . The upper limits of  $\zeta_2$  at 95% C.L. are obtained from the probabilistic distributions and are given in Table 2 as well.

Let us turn the attention to results in Table 2. In **METHOD A**, the tightest constraint is from PSR B2127+11C,  $|\zeta_2| < 3.1 \times 10^{-5}$  (95% C.L.). It is slightly better than Will’s result. For PSR B1913+16, our bound is  $|\zeta_2| < 1.2 \times 10^{-3}$  from **METHOD A**, which is about 30 times looser than the previous limit (Will 1992). The dominant reason for a worse result is the value of  $\ddot{P} \equiv -\dot{\nu}/\nu^2 + 2\dot{\nu}^2/\nu^3$ . Will (1992) used an unpublished value,  $\ddot{P} = 4 \times 10^{-30} \text{ s}^{-1}$ , which is actually more than an order of magnitude smaller than the recently published value in Weisberg & Huang (2016a),  $\ddot{P} = 5.6 \times 10^{-29} \text{ s}^{-1}$ . Such a difference is not surprising in the presence of red-noise processes, since the value of  $\dot{\nu}$  determined from timing data is likely to be affected by the time-span of the available data set (Hobbs et al. 2004). There is no simple relationship between the degree of variation of the actually measured  $\dot{\nu}$  value and the length of the timing data set, as higher order spin-frequency derivatives may be required additionally in order to describe the measured arrival times adequately (Hobbs et al. 2010). Red-noise processes also known as “timing noise” or “spin-noise”, affecting the measured spin-frequency derivatives, are common for young pulsars and may be related to the recovery from rotational instabilities known as “glitches” (Hobbs et al. 2010) or changes in the pulsar magnetosphere (Lyne et al. 2010). Red spin-noise is also expected to be common in recycled pulsars (Shannon & Cordes 2010), but evidently at a much smaller level (Hobbs et al. 2010; Lyne et al. 2010). Not many studies have espe-

**Table 2.** The bounds on the absolute value of  $\zeta_2$  from individual binary pulsar systems at 95% C.L.. We list the results in the order of  $\zeta_2$  bounds in **METHOD A**. The second column gives the quantity in deriving the constraint. The combined bounds from a Bayesian analysis can be found in Eqs. (10–13).

Pulsar		METHOD A	METHOD B
B2127+11C	$\dot{\nu}$	$3.1 \times 10^{-5}$	$2.9 \times 10^{-5}$
J1756–2251	$\dot{\nu}$	$1.7 \times 10^{-4}$	$1.8 \times 10^{-4}$
B1534+12	$\dot{\nu}$	$4.5 \times 10^{-4}$	$8.1 \times 10^{-5}$
B1913+16	$\ddot{\nu}$	$1.2 \times 10^{-3}$	$8.4 \times 10^{-4}$
B1534+12	$\ddot{\nu}$	$1.9 \times 10^{-3}$	$1.9 \times 10^{-3}$
B1913+16	$\dot{\nu}$	$4.1 \times 10^{-3}$	$1.5 \times 10^{-3}$

cially addressed the case of so-called “mildly recycled” pulsars which are studied here. However, the magnitude of  $\dot{\nu}$  values presented in Table 1 matches the expectation and general trends across the pulsar population (Hobbs et al. 2010).

Another reason is that we uniformly take the value of  $\omega(t)$  during the corresponding observational span. In Fig. 1, we notice that the value of  $\cos[\omega(t)]$  of PSR B1913+16 goes through zero, which could lead to a significant portion of samples of  $\zeta_2$  with nearly no constraint. Therefore, the distribution of  $\zeta_2$  has a very long tail. We have checked that, the limits at 68% C.L. are much smaller than half of the limits at 95% C.L., thus showing evidence of the non-Gaussian long tails in the posterior distribution. We have encountered a similar situation of long-tailed distributions for the test of PPN parameter  $\alpha_2$  (Shao & Wex 2012). The result from **METHOD B** also shows the evidence that we could get a better constraint,  $\zeta_2 < 8.4 \times 10^{-4}$ , when we use the value of  $\cos[\omega(t)]$  at the reference time  $t_0$  for PSR B1913+16, when  $\cos[\omega(t)]$  is different from zero. For these reasons, we treat the original limit from Will (1992) as an optimistic one, and ours more conservative.

In **METHOD A**, we have made an improvement in treating the changing  $\omega(t)$ . But for PSRs B1913+16 and B1534+12, their  $\cos[\omega(t)] \approx 0$  during some epoch. So **METHOD B** can provide a stronger limit than **METHOD A** for the two pulsars. For PSRs B2127+11C and J1756–2251, their values of  $\cos[\omega(t)]$  stayed away from zero during their observational spans, so **METHOD A** and **METHOD B** give similar results. In **METHOD B**, the best constraint comes from PSR B2127+11C,  $\zeta_2 < 2.9 \times 10^{-5}$  (95% C.L.). It is very close to the corresponding limit from **METHOD A**.

The bounds from  $\ddot{\nu}$  are also listed in Table 2 for PSRs B1913+16 and B1534+12. It is worth noting that, PSR B1913+16 can provide a better bound from  $\ddot{\nu}$  than from  $\dot{\nu}$ . It indicates that, at least for some pulsars,  $\ddot{\nu}$  can offer a stronger bound on  $\zeta_2$ . Therefore, if observers could publish

$\dot{\nu}$  and  $\ddot{\nu}$  parameters in the future, it will help to test the non-conservativeness of gravity theories.

### 3.3. A combined bound on $\zeta_2$

We can stack the posteriors from four pulsars to obtain a combined limit on  $\zeta_2$  via Monte Carlo simulations within the Bayesian framework, as suggested in the context of [Del Pozzo & Vecchio \(2016\)](#). In the Bayesian inference, given a prior, the posterior distribution of  $\zeta_2$  can be inferred with data,  $\mathcal{D}$ , and a hypothesis,  $\mathcal{H}$ . We use the Bayes' theorem,

$$P(\zeta_2|\mathcal{D}, \mathcal{H}, \mathcal{I}) = \int \frac{P(\mathcal{D}|\zeta_2, \Xi, \mathcal{H}, \mathcal{I}) P(\zeta_2, \Xi|\mathcal{H}, \mathcal{I})}{P(\mathcal{D}|\mathcal{H}, \mathcal{I})} d\Xi, \quad (8)$$

where  $\mathcal{I}$  denotes all other relevant knowledge, and  $\Xi$  collectively denotes all other unknown parameters. In the equation,  $P(\zeta_2|\mathcal{D}, \mathcal{H}, \mathcal{I})$  is an updated (marginalized) posterior distribution of  $\zeta_2$ ,  $P(\mathcal{D}|\zeta_2, \Xi, \mathcal{H}, \mathcal{I}) \equiv \mathcal{L}$  is the likelihood function,  $P(\zeta_2, \Xi|\mathcal{H}, \mathcal{I})$  is the prior on parameters  $\in \{\zeta_2, \Xi\}$ , and  $P(\mathcal{D}|\mathcal{H}, \mathcal{I})$  is the model evidence.

Before investigating the bound on  $\zeta_2$ , we construct the logarithmic likelihood function,

$$\ln \mathcal{L} = -\frac{1}{2} \sum \left[ \frac{\ddot{\nu}}{\sigma(\ddot{\nu}^{\text{upper}})} \right]^2 - \frac{1}{2} \sum \left[ \frac{\dot{\nu}}{\sigma(\dot{\nu}^{\text{upper}})} \right]^2, \quad (9)$$

where the  $\dot{\nu}$  and  $\ddot{\nu}$  in the numerator are the contributions from  $\zeta_2$  [cf. Eq. (4) and Eq. (7)], and the summations are over eligible systems (see below). The values of  $\sigma(\dot{\nu}^{\text{upper}})$  and  $\sigma(\ddot{\nu}^{\text{upper}})$  were discussed in Section 3.2.

Similarly, we investigate two scenarios. In the first scenario, we use binary pulsars with measured  $\dot{\nu}$  and/or  $\ddot{\nu}$ , and we utilize METHOD A for individual binary pulsar systems to deal with the time-varying  $\omega(t)$ . In the second scenario, we instead use METHOD B to obtain  $\omega(t)$ .

For the two scenarios above, for each we introduce two types of prior distribution for  $\zeta_2$ , namely a flat prior on  $\log_{10} |\zeta_2|$  in the range  $\log_{10} |\zeta_2| \in [-7, -3]$ , and a flat prior on  $\zeta_2$  in the range  $|\zeta_2| \in [10^{-7}, 10^{-3}]$ .

The posterior distributions with different priors are illustrated in Fig. 2 and Fig. 3 for METHOD A and METHOD B respectively. In METHOD A, the constraints at 95% C.L. are,

$$|\zeta_2| < 2.6 \times 10^{-5}, \quad \text{with flat prior in } \zeta_2, \quad (10)$$

$$|\zeta_2| < 1.3 \times 10^{-5}, \quad \text{with flat prior in } \log_{10} |\zeta_2|. \quad (11)$$

The bound in Eq. (11) improves the limit in [Will \(1992\)](#) by three time. In METHOD B, at 95% C.L. we have

$$|\zeta_2| < 2.7 \times 10^{-5}, \quad \text{with flat prior in } \zeta_2, \quad (12)$$

$$|\zeta_2| < 1.3 \times 10^{-5}, \quad \text{with flat prior in } \log_{10} |\zeta_2|. \quad (13)$$

That the two methods provide very close results proves the consistency and robustness of our approaches. In Table 2,

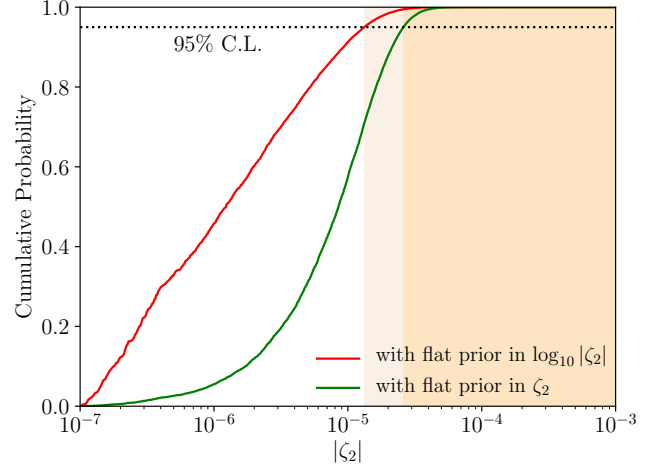


**Figure 2.** Cumulative posterior distributions with two different choices of priors, using the METHOD A for  $\omega(t)$ .

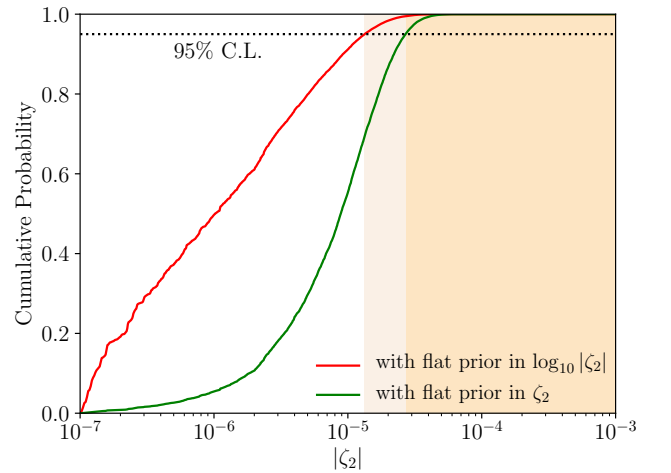


**Figure 3.** Same as Fig. 2, using METHOD B for  $\omega(t)$ .

except for PSR J1756–2251, METHOD B leads to a better constraint than METHOD A for individual bounds. But METHOD A gives similar result with METHOD B for the combined bound on  $\zeta_2$  with two different types of prior. The reason is related to the long tails of individual limits in METHOD A, when  $\cos \omega(t)$  crosses zero, as discussed above. When combining multiple distributions, the long tails are suppressed.

## 4. A FULL TIMING MODEL WITH SIMULATED DATA

In this section, we investigate the capability to limit  $\zeta_2$ , using simulations based on the observational characteristics of the chosen binary pulsars. In Section 4.1, we derive a new timing model with a non-zero  $\zeta_2$ . Then in Section 4.2 we use simulation of TOAs to investigate the capability to limit  $\zeta_2$  by the pulsar timing techniques. To mimic a usual fitting, we use polynomials of the time derivatives of the spin frequency at different orders to *absorb* the effect of  $\zeta_2$ .

**Table 3.** Relevant parameters for PSRs J0737–3039A (Kramer et al. 2006) and J1757–1854 (Cameron et al. 2018). Their  $\dot{\nu}$  was not reported in literature. Masses were obtained assuming the validity of GR. Parenthesized numbers represent the  $1\text{-}\sigma$  uncertainty in the last digit(s) quoted.

	PSR J0737–3039A	PSR J1757–1854
$t_0$ (MJD)	53156	57701
$T^{\text{obs}}$ (yr)	$\sim 2.67$	$\sim 1.6$
$\nu$ (Hz)	44.054069392744(2)	46.517617017655(15)
$\dot{\nu}$ ( $\text{s}^{-2}$ )	$-3.4156(1) \times 10^{-15}$	$-5.6917(15) \times 10^{-15}$
$\ddot{\nu}^{\text{dipole}}$ ( $\text{s}^{-3}$ )	$7.9 \times 10^{-31}$	$2.0 \times 10^{-30}$
$P_b$ (day)	0.10225156248(5)	0.18353783587(5)
$e$	0.0877775(9)	0.6058142(10)
$x_p$ (lt-s)	1.415032(1)	2.237805(5)
$\omega$ (deg)	87.0331(8)	279.3409(4)
$\dot{\omega}$ ( $\text{deg yr}^{-1}$ )	16.89947(68)	10.3651(2)
$m_p$ ( $M_\odot$ )	1.3381(7)	1.3384(9)
$m_c$ ( $M_\odot$ )	1.2489(7)	1.3946(9)
$q \equiv m_p/m_c$	1.0714(11)	0.9597(9)
$m$ ( $M_\odot$ )	2.58708(16)	2.73295(9)
$N_{\text{TOA}}$	131416	3162
$\sigma_{\text{TOA}}$ ( $\mu\text{s}$ )	54	36

We use six pulsars as examples. Four of them are given in Table 1, and additional two are listed in Table 3. We obtain the sensitivity to  $\zeta_2$  with current observational characteristics of six binary pulsars. For simplicity, for now we only consider white Gaussian noise in the simulation. Though it can be over-optimistic compared with the actual situation with red noise (see e.g. Caballero et al. 2016), our study provides a first demonstration of the full timing model, and a couple of useful clues for future investigation (cf. Section 4.3). A simple validation with real TOAs from PSR B1913+16 (Weisberg & Huang 2016a) supports our approach.

#### 4.1. Timing model with a non-zero $\zeta_2$

In pulsar timing, the difference between the predicted TOAs from a best-fit model and the measured TOAs is called the timing residual. If the timing residuals do not follow a Gaussian distribution with a mean of zero, it indicates that there is one or more physical factors which are probably not taken into account in the fitting (Lorimer & Kramer 2005). Therefore, if  $\zeta_2$  is large enough, it would lead to systematic deviations in the timing residuals from a zero-mean Gaussian distribution when it is not fully degenerate with existing timing parameters.

So far, for the six binary pulsars that we consider, they all nicely fit with the Damour-Deruelle (DD) timing model which is a phenomenological model for fully conservative

gravity theories and accounts for generic deviations from GR (Damour & Deruelle 1986; Damour & Taylor 1992). In other words, there are no obvious *non-conservative* effects of  $\zeta_2$  in the timing residuals. It means that, if  $\zeta_2 \neq 0$ , the value of  $\zeta_2$  is too tiny to be relevant, or its effects are possibly absorbed in other timing parameters, given the observational uncertainty. Here, we will use simulated TOAs with effects from  $\zeta_2$  included directly in the timing model, to investigate what value of  $\zeta_2$  can be visible.

First, we investigate how a non-zero  $\zeta_2$  will contribute to TOAs. It will automatically account for the linear-in-time evolution of  $\omega(t)$ . Extending the DD timing model (Damour & Deruelle 1985, 1986; Damour & Taylor 1992) we have,

$$t = T + \Delta_{\text{R}}(T) + \Delta_{\text{E}}(T) + \Delta_{\text{S}}(T) + \Delta_{\text{A}}(T) + \Delta_{\zeta_2}(T), \quad (14)$$

where  $T$  is the proper time of pulsar pulse emission, and  $t$  is the arrival time of pulses at the Solar system barycentre;  $\Delta_{\text{R}}(T)$  is the Roemer delay,  $\Delta_{\text{E}}(T)$  is the Einstein delay,  $\Delta_{\text{S}}(T)$  is the Shapiro delay, and  $\Delta_{\text{A}}(T)$  is the aberration delay (see Damour & Deruelle 1986, for details). The last term on the right-hand side of Eq. (14),  $\Delta_{\zeta_2}(T)$ , is the *perturbative* contribution from  $\zeta_2$ .

Now, we try to derive the concrete expression of  $\Delta_{\zeta_2}(T)$ . As given in Section 2, due to a violation of the conservation of energy-momentum via a non-zero  $\zeta_2$ , one has a self-acceleration,  $\mathbf{a}_{\text{cm}}$ , for the center of mass of a binary system (Will 1992). Its component along the line of sight is

$$a_r(t) \equiv \hat{\mathbf{n}} \cdot \mathbf{a}_{\text{cm}}(t) = \mathcal{A}_2 \sin[\omega_0 + \dot{\omega}(t - T_0)], \quad (15)$$

with  $T_0$  the epoch of periastron, and  $\omega_0$  the value of the longitude of periastron at  $T_0$ ;  $\mathcal{A}_2$  is given in Eq. (5). For simplicity, in the following we will take  $T_0 = t_0$  which is the reference epoch for the astrometric parameters.

For a pulsar in a binary system, the displacement  $z(t)$  along the line of sight, which is caused by the perturbative effects of  $\zeta_2$ , is determined via the relation  $\ddot{z}(t) = a_r(t)$ . After integration, we obtain

$$z(t) = \frac{\mathcal{A}_2}{\dot{\omega}^2} [\sin \omega_0 + \delta\omega \cos \omega_0 - \sin(\omega_0 + \delta\omega)], \quad (16)$$

where  $\delta\omega \equiv \dot{\omega}(t - t_0)$ . We have chosen  $z(t_0) = \dot{z}(t_0) = 0$  as the initial condition of integration. It is the most general choice, because other choices could always be absorbed into parameter redefinition. Due to a non-zero  $\zeta_2$ , the extra time delay of arrival of pulses can be described by,

$$\Delta_{\zeta_2} = z(t)/c \approx z(T)/c. \quad (17)$$

Here, the difference between  $T$  and  $t$  is at higher orders and we will neglect it. The above equation could be directly applied in pulsar timing softwares, e.g. TEMPO. We have implemented such a timing model with  $\zeta_2$  (see below).



To comply with the tests utilizing  $\dot{\nu}$  and  $\ddot{\nu}$  that we mentioned in Section 3, we apply Taylor expansion to  $\Delta_{\zeta_2}$  with respect to  $T - t_0$ ,

$$\begin{aligned} \Delta_{\zeta_2}(T) = & \frac{1}{2} \frac{\mathcal{A}_2}{c} \sin \omega_0 (T - t_0)^2 + \frac{1}{6} \frac{\mathcal{A}_2 \dot{\omega}}{c} \cos \omega_0 (T - t_0)^3 \\ & - \frac{1}{24} \frac{\mathcal{A}_2 \dot{\omega}^2}{c} \sin \omega_0 (T - t_0)^4 + \dots \end{aligned} \quad (18)$$

As we can imagine,  $\Delta_{\zeta_2}$  would cause the *observed* spin frequency  $\nu$  to change as a function of time.

On the other hand, from pulsar astronomy we have the rotational phase of a pulsar as a Taylor expansion (Lorimer & Kramer 2005),

$$\begin{aligned} \phi(T) = & \phi_0 + \nu(T - t_0) + \frac{1}{2} \dot{\nu}(T - t_0)^2 + \frac{1}{6} \ddot{\nu}(T - t_0)^3 \\ & + \frac{1}{24} \ddot{\nu}(T - t_0)^4 + \dots \end{aligned} \quad (19)$$

Comparing Eq. (18) with Eq. (19), the PPN  $\zeta_2$  will contribute to the time derivatives of the pulsar spin in the TOA fitting, namely some effects are degenerate. For the extra time delay that is caused by an *apparent* change in the spin frequency, we have  $-\Delta_{\zeta_2} = \delta\phi/P = \delta\phi/\nu$ , and

$$\delta\phi = \frac{1}{2} \delta\dot{\nu}(T - t_0)^2 + \frac{1}{6} \delta\ddot{\nu}(T - t_0)^3 + \frac{1}{24} \delta\ddot{\nu}(T - t_0)^4 + \dots \quad (20)$$

Consequently, we have the following relations for the extra time delay caused by  $\zeta_2$ ,

$$-\frac{\mathcal{A}_2 \dot{\omega}}{c} \cos \omega_0 = \delta\dot{\nu}/\nu, \quad (21)$$

$$\frac{\mathcal{A}_2 \dot{\omega}^2}{c} \sin \omega_0 = \delta\ddot{\nu}/\nu. \quad (22)$$

They are actually equivalent to Eq. (4) and Eq. (7). If there is only the  $\zeta_2$  parameter contributing to  $\delta\dot{\nu}$  and  $\delta\ddot{\nu}$ , Eqs. (21) and (22) can be made use of to test  $\zeta_2$ . Notice that, we do not consider a possible constraint from  $\delta\dot{\nu}$ , because this parameter is much more likely to be dominated by un-modeled astrophysical processes (for example, by the dipole radiation of pulsars), thus  $\dot{\nu}$  can provide a more reasonable constraint than  $\dot{\nu}$  (Will 1992). As in Section 3, we will only consider  $\ddot{\nu}$  and  $\ddot{\nu}$  in the following.

#### 4.2. Simulations and fitting to TOAs

In order to investigate the capability to limit  $\zeta_2$  with binary pulsars, we construct simulated TOAs including the effect of  $\zeta_2$ . For simplicity, we assume that, the contribution from a non-zero, yet small,  $\zeta_2$  does not significantly affect the best-fitting parameters from pulsar timing. We use the published parameters that were obtained without considering the time delay effect of  $\zeta_2$ . These parameters are given in Tables 1

and 3. By doing this, we are assuming that the effects from  $\zeta_2$  are perturbatively small. We consider such an assumption reasonable at the stage of *bounding*  $\zeta_2$  instead of *measuring* it. In addition, we only assume white Gaussian noise in our simulation. There could be heterogeneous noise and significant red noise for some binary pulsars (Caballero et al. 2016). We feel the assumption of white noise to be optimistic, but still reasonable, for this *demonstrative* study. Further studies can be conducted to investigate the effects from red noise and more realistic observational cadence.

For each pulsar, we simulate TOAs,  $\{t_n\}_{n=1}^{N_{\text{TOA}}}$ , where  $N_{\text{TOA}}$  is the number of TOAs which were used to derive the actual pulsar parameters (see the penultimate row in Tables 1 and 3). Simplifying the actual observational cadence, here the  $n$ -th simulated TOA is expressed as  $t_n = n T^{\text{obs}}/N_{\text{TOA}}$ , namely, they are chosen to be uniform in the observational span  $T^{\text{obs}}$ . We utilize their root mean square (RMS) residual, given in the last row of Tables 1 and 3, to generate the white timing noise,  $w(t_n)$ . We add randomly generated noise to these TOAs. On top of these fake TOAs, we add the timing delay caused by a non-zero  $\zeta_2$ ,  $\Delta_{\zeta_2}(T)$ , which is directly obtained from Eq. (17).

Now we try to extract the  $\zeta_2$  parameter from simulated timing residuals. In our investigation, given a realization of  $\{t_n\}$  and a value of  $\zeta_2^{\text{input}}$ , we can simulate timing residuals for each pulsar based on their timing parameters in Tables 1 and 3. With these simulated timing residuals, we try to separate the effect of  $\zeta_2$ , with a simplified timing model. To mimic the fitting in real situation, we use a polynomial that is expanded with respect to  $T - t_0$ ,

$$\Delta(T) = \frac{1}{2} \alpha (T - t_0)^2 + \frac{1}{6} \beta (T - t_0)^3 + \frac{1}{24} \gamma (T - t_0)^4 + \dots, \quad (23)$$

where  $\alpha$ ,  $\beta$ , and  $\gamma$  are all fitting parameters.

When comparing Eqs. (18) and (23), we observe the following correspondence:  $\alpha = \mathcal{A}_2 \sin \omega_0/c$ ,  $\beta = \mathcal{A}_2 \dot{\omega} \cos \omega_0/c$  and  $\gamma = -\mathcal{A}_2 \dot{\omega}^2 \sin \omega_0/c$ . These parameters are treated independently in the fitting, therefore we will put a superscript to indicate the order of the corresponding polynomial coefficients hereafter. As we have discussed before, due to the contamination in  $\dot{\nu}$  (Will 1992), we only utilize the fitting parameters  $\beta$  and  $\gamma$  to derive bounds on  $\zeta_2$ . In fact, according to Eqs. (21) and (22),  $\beta$  and  $\gamma$  are related to the usual  $\dot{\nu}$  and  $\ddot{\nu}$ , respectively. As the result of fitting, the derived  $\zeta_2$ , which we denote as  $\zeta_2^{\text{fit}}$ , can be obtained from the coefficients at different orders,  $\mathcal{A}_2^{(3)}$  and  $\mathcal{A}_2^{(4)}$ .

In order to investigate at which level we will be able to bound  $\zeta_2$ , we fit the simulated timing residuals with Eq. (23) according to the following two schemes. In the first scenario, we fit the timing residuals with Eq. (23) up to the *third* order, namely by including  $\alpha$  and  $\beta$ . We derive the value of  $\zeta_2^{\text{fit}}$  from  $\beta$ . For convenience, we call it METHOD I. In the second

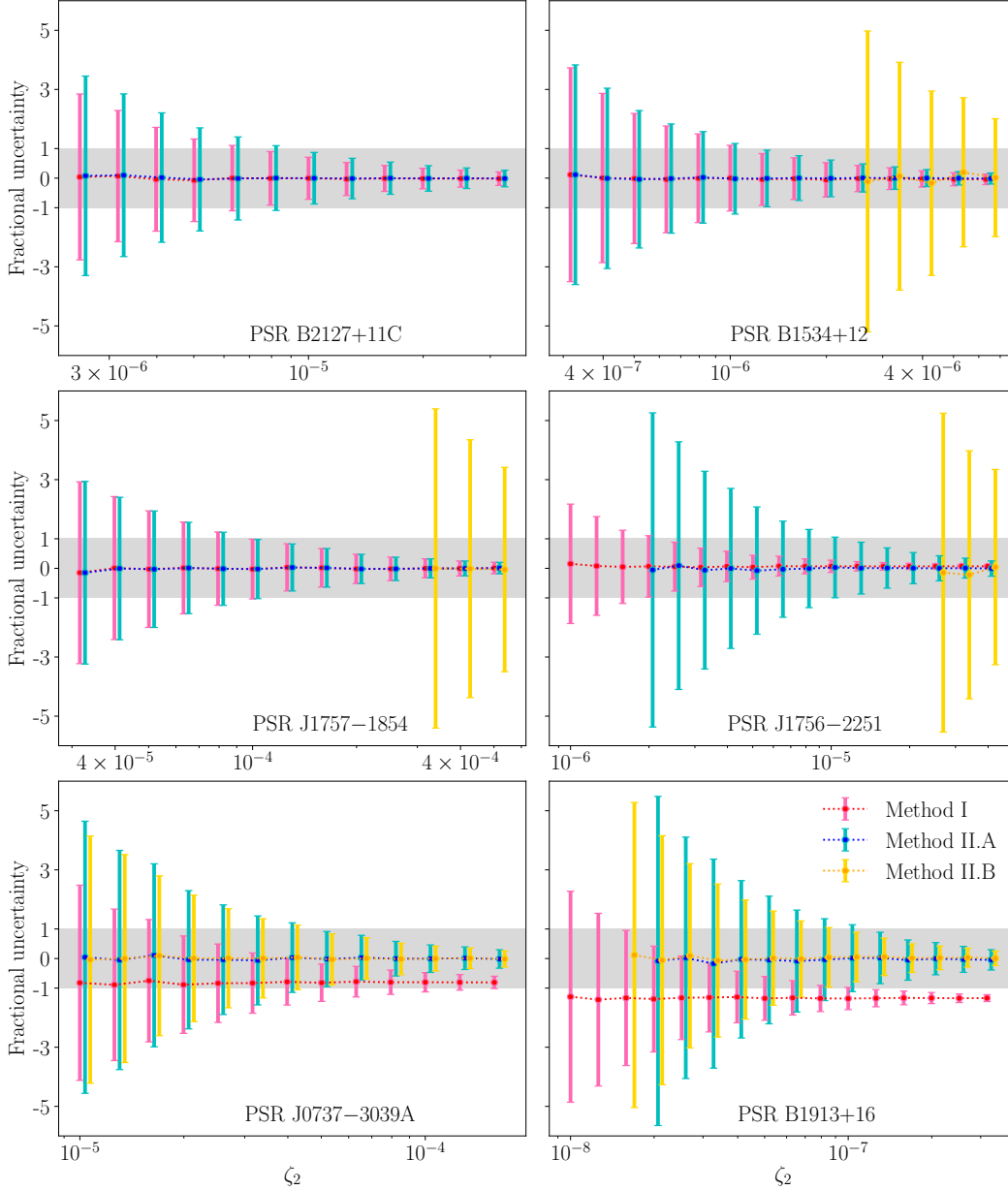


**Figure 4.** Fractional uncertainties  $\mathcal{R}$  for six binary pulsars from three different methods, as a function of  $\zeta_2^{\text{input}}$  (see text for more details). The gray strip is a region which is bound by  $\sigma(\mathcal{R}) \leq 1$ . When  $\sigma(\mathcal{R})$  is smaller than the width of the gray strip, the effect from  $\zeta_2$  starts to be relevant.

scenario, we fit the timing residuals with Eq. (23) up to the *fourth* order, namely by including  $\alpha$ ,  $\beta$ , and  $\gamma$ . Differently from the previous scenario, now in principle we can obtain two independent bounds on  $\zeta_2$  from either  $\beta$  or  $\gamma$ . To make a clear distinction, the methods where  $\zeta_2^{\text{fit}}$  is derived from  $\mathcal{A}_2^{(3)}$  and  $\mathcal{A}_2^{(4)}$  are named as METHOD II.A and METHOD II.B, respectively. Worth to note that, in the case that we can contribute  $\ddot{v}$  and  $\ddot{v}$  solely to  $\zeta_2$ , if METHOD II.A and METHOD II.B give a same value of  $\zeta_2$ , it represents a way to *detect*  $\zeta_2$  other than to *bound*  $\zeta_2$ . But in reality, it might be difficult to separate other astrophysical contributions to  $\ddot{v}$  and  $\ddot{v}$ .

Until now, we have introduced how to derive  $\zeta_2^{\text{fit}}$  with a realization of the white noise  $w(t_n)$  and a non-zero  $\zeta_2^{\text{input}}$  for a pulsar. Because of the existence of random noise, given a  $\zeta_2^{\text{input}}$ ,  $\zeta_2^{\text{fit}}$  inherits the randomness. Therefore we generate a set of realization of  $w(t_n)$  and repeat the simulations and fittings to obtain statistical distributions for  $\zeta_2^{\text{fit}}$ .

To quantify the difference between  $\zeta_2^{\text{input}}$  and  $\zeta_2^{\text{fit}}$ , we introduce the fractional uncertainty,  $\mathcal{R} \equiv (\zeta_2^{\text{fit}} - \zeta_2^{\text{input}}) / \zeta_2^{\text{input}}$ . For each pulsar, we record the distribution of  $\zeta_2^{\text{fit}}$ , and obtain the distribution of  $\mathcal{R}$  from it. The mean of the distribution of  $\mathcal{R}$  is expected to be zero for *unbiased* fittings. The timing residual

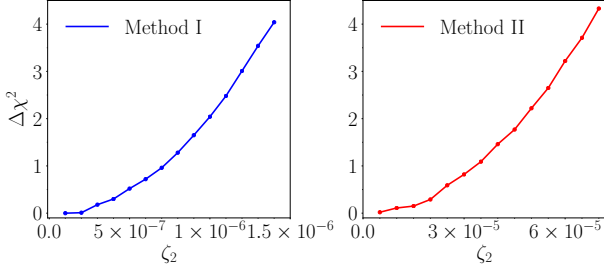


**Figure 5.** Changes in the  $\chi^2$  as a function of  $\zeta_2$  for PSR B1913+16.

from  $\zeta_2$  is included in fake TOAs via Eq. (17), while it is fit via Eq. (23). Therefore, intrinsically, we are biased. But as we will see later, such a bias is not important for most of our binary pulsars.

The  $1\text{-}\sigma$  uncertainty of  $\mathcal{R}$ , denoted as  $\sigma(\mathcal{R})$ , describes the pulsar’s capability to limit  $\zeta_2$ . When  $\sigma(\mathcal{R}) > 1$ , we consider that the effects of  $\zeta_2^{\text{input}}$  are buried in noise and cannot be extracted. For the following, we introduce  $\sigma(\mathcal{R}) \leq 1$  as a criterion for detectability. For each pulsar, we repeat the above processes for multiple values of  $\zeta_2^{\text{input}}$ , to look for the critical value, which is the smallest value of  $\zeta_2^{\text{input}}$  that meets the criterion. For the binary pulsars that we use, we investigate proper ranges of  $\zeta_2^{\text{input}}$  for each pulsar individually. With METHOD I, METHOD II.A, and METHOD II.B, we obtain the value of  $\mathcal{R}$  and  $\sigma(\mathcal{R})$  as a function of  $\zeta_2^{\text{input}}$ . The results are illustrated in Fig. 4 for the six chosen pulsars. The critical values of  $\zeta_2^{\text{input}}$  for  $\sigma(\mathcal{R}) = 1$  are collected in Table 4.

To have a better sense of implementation, we augment the DD timing model with the extra time delay in Eq. (17) in the TEMPO software. Using the full timing model in TEMPO we have verified the simplified treatments above. In addition, we apply the new model to the public data of PSR B1913+16 (Weisberg & Huang 2016a) from real observations. Instead of fitting  $\zeta_2$  directly, we scan the values of  $\zeta_2$  in appropriate ranges and record the changes in  $\chi^2$ . Same as the analysis in this subsection, we freely fit for up to the second time derivative of the spin frequency in METHOD I, and up to the third time derivative of the spin frequency in METHOD II. Our results are plotted in Fig. 5. As we can see, though the cadence of real data is very different from our simulation, the results are consistent with our analysis. Worth to note that, in the fitting of Weisberg & Huang (2016b), higher time derivatives of the spin frequency were used. These parameters are not free in the calculation of Fig. 5 for simplicity. These higher frequency derivatives might be caused by red noise. In contrast to this demonstrative work, they need to be properly accounted for in real data analysis.

### 4.3. Discussions

Now, we analyze and discuss the implication of our results in the Fig. 4 and Table 4. Naturally, as one can see in Fig. 4, when  $\zeta_2^{\text{input}}$  increases, the signal gets more prominent

and the fractional uncertainty in estimating  $\zeta_2$  gets smaller. It becomes easier to separate the  $\zeta_2$  effect from other noise given by the RMS timing residuals. It indicates a stronger capability to limit  $\zeta_2$ .

As we also observe in Fig. 4, except for PSRs J0737–3039A and B1913+16, when  $\zeta_2^{\text{input}}$  increases, the mean of  $\mathcal{R}$  gradually converges to zero with METHOD I. It means that, though the  $\zeta_2$  effects are introduced through the full timing model in Eq. (17), the fitting using Eq. (23) with polynomial coefficients  $\alpha$  and  $\beta$  are enough to *absorb* the residuals, effectively into the spin-down/spin-up parameters. But for PSRs B1913+16 and J0737–3039A, the  $\zeta_2$  effects cannot be absorbed solely with  $\alpha$  and  $\beta$ ; the recovery will be biased if only  $\alpha$  and  $\beta$  are used. Nevertheless, if we have included the  $\gamma$  coefficient in Eq. (23), as shown with METHOD II.A and METHOD II.B, the  $\zeta_2$  effects can be almost totally absorbed.

For a larger value of  $\zeta_2^{\text{input}}$ , it is easier to identify the  $\zeta_2$  parameter with the pulsar timing data. In our criterion, if  $\zeta_2^{\text{input}} < \zeta_2^{\text{crit}}$ , the effects of  $\zeta_2$  are buried underneath white noise. When  $\zeta_2^{\text{input}} > \zeta_2^{\text{crit}}$ , we consider that we are able to notice the  $\zeta_2$  effect via pulsar timing. Hence, we take  $\zeta_2^{\text{crit}}$  of a pulsar as its measure of the capability to limit  $\zeta_2$ . The values of  $\zeta_2^{\text{crit}}$  with different methods are listed in Table 4. It should be noted that, in the simulation we have used a uniform cadence and do not consider red noise, so the results from our simulation should be considered as optimistic estimates. Our main purpose with this section is to illustrate the timing formalism and simply indicate its possible use in the future.

Nevertheless, we would like to extract some useful clues for future studies. According to the different behaviors in the convergence of the quantity  $\mathcal{R}$  in Fig. 4, We divide the six binary pulsars into three categories for discussions.

- In the first category, we have PSRs B1534+12, B2127+11C and J1757–1854. As shown in Fig. 4, for each of these three pulsars, METHOD I and METHOD II.A have a similar capability to limit  $\zeta_2$ , while METHOD II.B performs much worse. Especially, for PSR B2127+11C, its  $\zeta_2^{\text{crit}}$  from METHOD II.B,  $\zeta_2^{\text{crit}} = 7.0 \times 10^{-3}$ , is too large and exceeds the plot range of the vertical axis.
- In the second category, we have PSR J1756–2251. For this pulsar, METHOD I provides a tighter result than METHOD II.A and METHOD II.B. We notice that in the fitting the coefficients  $\beta$  and  $\gamma$  are highly correlated, which worsens the tests with METHOD II.A and METHOD II.B.
- In the third category, we have PSRs B1913+16 and J0737–3039A, whose central values of  $\mathcal{R}$  from METHOD I deviate significantly from zero. Instead,

**Table 4.** Critical values of  $\zeta_2$  for six binary pulsars with three different methods. Corresponding values of  $\dot{\nu}$  and  $\ddot{\nu}$  are listed next to them. METHOD I for PSRs B1913+16 and J0737–3039A is biased (see Fig. 4), thus not listed.

	METHOD I		METHOD II.A		METHOD II.B	
	$\zeta_2^{\text{crit}}$	$\dot{\nu}$ (Hz <sup>3</sup> )	$\zeta_2^{\text{crit}}$	$\dot{\nu}$ (Hz <sup>3</sup> )	$\zeta_2^{\text{crit}}$	$\ddot{\nu}$ (Hz <sup>4</sup> )
B1534+12	$1.2 \times 10^{-6}$	$-4.9 \times 10^{-31}$	$1.2 \times 10^{-6}$	$-4.9 \times 10^{-31}$	$1.2 \times 10^{-5}$	$-2.0 \times 10^{-38}$
J0737–3039A	–	–	$4.4 \times 10^{-5}$	$2.3 \times 10^{-27}$	$3.4 \times 10^{-5}$	$-3.2 \times 10^{-34}$
J1756–2251	$2.0 \times 10^{-6}$	$5.3 \times 10^{-29}$	$1.1 \times 10^{-5}$	$2.9 \times 10^{-28}$	$1.3 \times 10^{-4}$	$3.1 \times 10^{-36}$
J1757–1854	$1.0 \times 10^{-4}$	$-2.8 \times 10^{-26}$	$1.0 \times 10^{-4}$	$-2.8 \times 10^{-26}$	$1.7 \times 10^{-3}$	$-1.7 \times 10^{-32}$
B2127+11C	$7.0 \times 10^{-6}$	$8.5 \times 10^{-29}$	$8.0 \times 10^{-6}$	$9.7 \times 10^{-29}$	$7.0 \times 10^{-3}$	$5.5 \times 10^{-35}$
B1913+16	–	–	$1.0 \times 10^{-7}$	$2.1 \times 10^{-30}$	$8.0 \times 10^{-8}$	$9.5 \times 10^{-39}$

when we use METHOD II.A or METHOD II.B, the recovered  $\zeta_2$  is not biased from  $\zeta_2^{\text{input}}$  at large. The results urge us to include the contribution from at least up to the fourth order of  $T - t_0$  in Eq. (23) when we use it to mimic the contribution from  $\zeta_2$  [cf. Eq. (17)] for PSRs B1913+16 and J0737–3039A. In addition, for these two pulsars, METHOD II.B provides a smaller  $\zeta_2^{\text{crit}}$  than METHOD II.A. Therefore,  $\ddot{\nu}$ , instead of  $\dot{\nu}$ , will provide a stronger test of  $\zeta_2$  with their observational characteristics. This is likely caused by the fact that PSR J0737–3039A has an extraordinarily large  $\dot{\omega} \simeq 17^\circ \text{yr}^{-1}$ , while PSR B1913+16 has been observed from several decades. It also confirms our conjecture in Section 3.2, that the bound on  $\zeta_2$  from  $\ddot{\nu}$  might be stronger than that from  $\dot{\nu}$  for some binary pulsar systems. It will be important if we want to apply the timing model (17) to the new data of Double Pulsar (Kramer et al. in preparation).

In our simulation for PSR J0737–3039A, we have used the observational characteristics in Kramer et al. (2006). The observational span was  $T^{\text{obs}} \lesssim 3 \text{ yr}$  and now the pulsar has been monitored for a much longer time span. Therefore, it is interesting to investigate its current ability in bounding  $\zeta_2$ . We simulate additional TOAs for  $\sim 17 \text{ yr}$  using the same observational cadence and the same level of RMS noise as in Kramer et al. (2006). We find that under white Gaussian noise and uniform observational cadence, it is able to probe  $\zeta_2$  at the level of  $\mathcal{O}(10^{-8})$ . If Taylor-expanded polynomials are used, higher-order terms are needed for an unbiased parameter recovery, as its  $\omega$  has changed by  $\sim 200^\circ$  over this time-span of observation. A publication for a new test of  $\zeta_2$  with real decade-long timing data for PSR J0737–3039A is under plan.

## 5. SUMMARY

Conservation of energy and momentum is an important property of a gravity theory. In the PPN framework, the

PPN parameter  $\zeta_2$  describes a class of theories that violate the conservation laws (Will 2018). There are explicit examples for this kind of theories (Rastall 1972; Smalley 1975), where the divergence of the energy-momentum tensor does not vanish [see e.g. Eq. (9) in Smalley (1975)]. The PPN parameter  $\zeta_2$  is proportional to this non-vanishing divergence [see Eq. (43) in Smalley (1975)]. Therefore, a generic bound on  $\zeta_2$  can be translated to a bound on the divergence of the energy-momentum tensor in these theories. A non-zero  $\zeta_2$  leads to characteristic timing behaviors for a pulsar in the binary, which can be tested via observations (Will 1992). In our study, we systematically investigate possible bounds on the  $\zeta_2$  parameter with updated timing solutions for four binary pulsars, utilizing the time derivatives of their spin frequency.

First, we carefully choose four binary pulsar systems, and for each pulsar we use the method of Will (1992) to put an individual bound on  $\zeta_2$ . To improve the choice of a time-dependent  $\omega(t)$ , we adopt two methods. In both methods, PSR B2127+11C provides a stronger bound than that in Will (1992). For PSR B1913+16, the result is about 30 times looser than the previous limit. The loose bound of PSR B1913+16 is due to a larger  $\dot{P}$  (or equivalently,  $\dot{\nu}$ ) than the one Will used, as well as the resultant distribution of  $\zeta_2$  with a non-Gaussian long tail from the crossing of zero for  $\cos[\omega(t)]$ .

Then, we extend the method in Will (1992) to investigate the relation between  $\ddot{\nu}$  and  $\zeta_2$ . We have access to  $\ddot{\nu}$  for PSRs B1913+16 and B1534+12. From PSR B1913+16, we obtain a stronger bound from  $\ddot{\nu}$  rather than  $\dot{\nu}$ , indicating that  $\ddot{\nu}$  could give a tighter bound for some binary pulsars. It is consistent with simulations in Section 4 using a set of completely different methods. Therefore, we urge observers to publish more frequency derivatives in order to conduct interesting gravity tests.

To use the maximum potential of an ensemble of pulsars, we derive bounds on  $\zeta_2$  by combining four binary pulsars within the Bayesian framework. We obtain, using a flat prior

for  $\log_{10} |\zeta_2| \in [-7, -3]$ ,

$$|\zeta_2| < 1.3 \times 10^{-5} \quad (95\% \text{ C.L.}), \quad (24)$$

which improves the result of Will (1992) by a factor of three.

In addition to using  $\dot{\nu}$  and  $\ddot{\nu}$ , we explore  $\zeta_2$ 's direct effect in the timing data. We develop a full timing model that includes the effects of  $\zeta_2$ , and implement it in the TEMPO software. We simulate timing residuals for six binary pulsars with their observational characteristics as input (including RMS timing residuals, number of TOAs and so on). For each pulsar we obtain their capability to limit  $\zeta_2$ , represented by a critical value,  $\zeta_2^{\text{crit}}$ . Using our criterion that the  $\zeta_2$  signal is not buried in noise, for each pulsar we use three methods to derive  $\zeta_2^{\text{crit}}$ , which represents a lower limit for  $\zeta_2$  in order to be detected. When  $\zeta_2$  is smaller than  $\zeta_2^{\text{crit}}$ , it is impossible to measure  $\zeta_2$  due to the presence of timing noise. In our simulation, we have assumed white noise and a uniform observational cadence. These assumptions have rendered our results quite optimistic ones. Nevertheless, as the first study, it concludes some useful clues in using the timing delay from  $\zeta_2$  for future real data analysis. For example, the simulations of PSRs B1913+16 and J0737–3039A show (i) the necessity to include higher-order time derivatives of the spin frequency if a polynomial functional is used to mimic the  $\zeta_2$  effect, and

(ii) the potential that  $\ddot{\nu}$  could provide a tighter bound on  $\zeta_2$  other than  $\dot{\nu}$ . As now we have a full timing model, in the future, instead of using frequency derivatives, one can in principle use the full timing model, in combination with red noise modeling to test the PPN  $\zeta_2$  parameter.

We thank Clifford Will and Heng Xu for helpful discussions. We are grateful to Robert Ferdman, Paulo Freire, Vivek Venkatraman Krishnan, and Alessandro Ridolfi for private communication, and Paulo Freire for carefully reading the manuscript. This work was supported by the National Natural Science Foundation of China (11975027, 11991053, 11721303), the Young Elite Scientists Sponsorship Program by the China Association for Science and Technology (2018QNRC001), and the Max Planck Partner Group Program funded by the Max Planck Society. LS, NW and MK acknowledge support from the European Research Council (ERC) via the ERC Synergy Grant BlackHoleCam under Contract No. 610058. The work was partially supported by the Strategic Priority Research Program of the Chinese Academy of Sciences through the Grant No. XDB23010200, and the High-performance Computing Platform of Peking University.

*Software:* TEMPO (Nice et al. 2015)

## REFERENCES

- Berti, E., et al. 2015, *Class. Quant. Grav.*, 32, 243001
- Caballero, R. N., et al. 2016, *Mon. Not. Roy. Astron. Soc.*, 457, 4421
- Cameron, A. D., et al. 2018, *Mon. Not. Roy. Astron. Soc.*, 475, L57
- Chadwick, J. 1932, *Nature*, 129, 312
- Cowan, C. L., Reines, F., Harrison, F. B., Kruse, H. W., & McGuire, A. D. 1956, *Science*, 124, 103
- Damour, T., & Deruelle, N. 1985, *AHHPA*, 43, 107
- . 1986, *AHHPA*, 44, 263
- Damour, T., & Esposito-Farèse, G. 1992, *Phys. Rev. D*, 46, 4128
- Damour, T., & Taylor, J. H. 1992, *Phys. Rev. D*, 45, 1840
- Del Pozzo, W., & Vecchio, A. 2016, *Mon. Not. Roy. Astron. Soc.*, 462, L21
- Ferdman, R. D., et al. 2014, *Mon. Not. Roy. Astron. Soc.*, 443, 2183
- Finn, L. S., & Sutton, P. J. 2002, *Phys. Rev. D*, 65, 044022
- Fonseca, E., Stairs, I. H., & Thorsett, S. E. 2014, *Astrophys. J.*, 787, 82
- Freire, P. C. C., Wex, N., Esposito-Farèse, G., et al. 2012, *Mon. Not. Roy. Astron. Soc.*, 423, 3328
- Freire, P. C. C., Ridolfi, A., Kramer, M., et al. 2017, *Mon. Not. Roy. Astron. Soc.*, 471, 857
- Hobbs, G., Lyne, A. G., & Kramer, M. 2010, *Mon. Not. Roy. Astron. Soc.*, 402, 1027
- Hobbs, G., Lyne, A. G., Kramer, M., Martin, C. E., & Jordan, C. 2004, *Mon. Not. Roy. Astron. Soc.*, 353, 1311
- Hulse, R. A., & Taylor, J. H. 1975, *Astrophys. J.*, 195, L51
- Jacoby, B. A., Cameron, P. B., Jenet, F. A., et al. 2006, *Astrophys. J.*, 644, L113
- Joshi, K. J., & Rasio, F. A. 1997, *Astrophys. J.*, 479, 948
- Kramer, M., et al. 2006, *Science*, 314, 97
- Lorimer, D. R., & Kramer, M. 2005, *Handbook of Pulsar Astronomy* (Cambridge, England: Cambridge University Press)
- Lyne, A., Hobbs, G., Kramer, M., Stairs, I., & Stappers, B. 2010, *Science*, 329, 408
- Mamajek, E. E., et al. 2015, arXiv:1510.07674
- Manchester, R. N. 2015, *Int. J. Mod. Phys. D*, 24, 1530018
- Manchester, R. N., Hobbs, G. B., Teoh, A., & Hobbs, M. 2005, *Astron. J.*, 129, 1993
- Miao, X., Shao, L., & Ma, B.-Q. 2019, *Phys. Rev. D*, 99, 123015
- Nice, D., Demorest, P., Stairs, I., et al. 2015, *Tempo: Pulsar timing data analysis*, *Astrophysics Source Code Library*, ascl:1509.002. <http://ascl.net/1509.002>
- Nordtvedt, K. 1987, *Astrophys. J.*, 320, 871
- Rastall, P. 1972, *Phys. Rev. D*, 6, 3357

- Shannon, R. M., & Cordes, J. M. 2010, *Astrophys. J.*, 725, 1607
- Shao, L. 2014a, *Phys. Rev. Lett.*, 112, 111103
- . 2014b, *Phys. Rev. D*, 90, 122009
- Shao, L., & Bailey, Q. G. 2018, *Phys. Rev. D*, 98, 084049
- Shao, L., Caballero, R. N., Kramer, M., et al. 2013, *Class. Quant. Grav.*, 30, 165019
- Shao, L., & Wex, N. 2012, *Class. Quant. Grav.*, 29, 215018
- . 2016, *Sci. China Phys. Mech. Astron.*, 59, 699501
- Smalley, L. L. 1975, *Phys. Rev. D*, 12, 376
- Stairs, I. H. 2003, *Living Rev. Rel.*, 6, 5
- Taylor, J. H. 1992, *Phil. Trans. A. Math. Phys. Eng. Sci.*, 341, 117
- Taylor, J. H., Fowler, L. A., & McCulloch, P. M. 1979, *Nature*, 277, 437
- van Leeuwen, J., et al. 2015, *Astrophys. J.*, 798, 118
- Weisberg, J., & Huang, Y. 2016a, Zenodo.  
<https://doi.org/10.5281/zenodo.54764>
- Weisberg, J., Stanimirovic, S., Xilouris, K., et al. 2008, *Astrophys. J.*, 674, 286
- Weisberg, J. M., & Huang, Y. 2016b, *Astrophys. J.*, 829, 55
- Wex, N. 2014, in *Frontiers in Relativistic Celestial Mechanics: Applications and Experiments*, ed. S. M. Kopeikin, Vol. 2 (Walter de Gruyter GmbH, Berlin/Boston), 39
- Will, C. M. 1976, *Astrophys. J.*, 205, 861
- Will, C. M. 1992, *Astrophys. J. Lett.*, 393, L59
- Will, C. M. 2014, *Living Rev. Rel.*, 17, 4
- . 2018, *Theory and Experiment in Gravitational Physics* (Cambridge University Press)